Fibers and Polymers (2024) 25:2117–2130
https://doi.org/10.1007/s12221-024-00584-7

Online ISSN 1875-0052
Print ISSN 1229-9197

REGULAR ARTICLE

Influence of Supercritical Carbon Dioxide-Assisted Polyamide Acid Modification of Aramid Fibers on the Properties of Aramid Fiber-Reinforced Styrene Butadiene Rubber

Yang Li[1,2] · Caiwen Shi[1,2] · Xiaoli Pan[1,2] · Le Yang[1,2]

Received: 2 November 2023 / Revised: 28 April 2024 / Accepted: 9 May 2024 / Published online: 22 May 2024

Abstract
Modified aramid fibers (AFs) were prepared through grafting modification of polyamide acid (PAA) assisted by supercritical carbon dioxide ($scCO_2$). The $scCO_2$-assisted diffusion, penetration, and grafting reaction of PAA not only enhanced the graft rate but also produced a uniformly grafted layer on the modified fibers. After $scCO_2$-assisted grafting with 5 wt% PAA, the grafted amount was 10.23%, the surface crystal spacing increased, and the crystallinity increased by 8.64%. Moreover, the tensile strength of the uniformly layered fibers increased by 9.66%. Next, short modified AF-reinforced carbon black/styrene butadiene rubber (SBR) was prepared with an AF/CB/SBR ratio of 2/50/100 parts per hundred rubber. As an acidic substance in the grafted coating layer, PAA was found to delay the vulcanization process and increase the positive vulcanization time. After modification with $scCO_2$-assisted 5 wt% PAA, the –COOH groups in the grafted layer participated in the curing process of the curing agent. The rough and uniformly grafted layer enhanced the dispersibility of the modified fibers through the SBR matrix. The modification increased the tensile strength and modulus at 100% of the composites by 16.01 and 32.47% and accordingly improved the cutting resistance.

Keywords Aramid fiber · Polyamide acid · Supercritical carbon dioxide · Styrene butadiene rubber · Interfacial bonding

1 Introduction

Owing to its excellent wear resistance, heat resistance, and global abundance, styrene butadiene rubber (SBR) is widely used in the tire industry, wire and cable products, medical appliances, and various rubber products [1, 2]. Carbon black (CB) which is widely used as a reinforcing material for SBR can condense into the network structure in vulcanized composites and provide reinforcing effect [3, 4]. Unfortunately, for the vulcanization rubber system reinforced only by carbon black, the desorption of CB could cause the decrease of rubber cross-linking density and modulus at large deformation, which weakened the anti-puncture and anti-fatigue ability of the products [5]. The short fiber-reinforced rubber (SFRR) composites can combine the high elasticity of rubber and the rigidity of fiber well, which made a significant contribution to high tearing strength and anisotropic properties [6, 7].

Previous studies have shown that aramid fiber (AF) exerts the best strengthening effect on natural rubber [2] and SBR [4, 5]. Short AFs can synergize with inorganic particles such as CB to improve the critical strain of Payne, obtaining high-performance SFRR materials for engineering applications. However, interactions between the amide bond and other groups are inhibited by the shielding effect of the benzene ring, so the AFs insufficiently adhere to the rubber matrix [2, 4, 5]. Improving the interfacial bonding between modified AFs and SBR is currently the main challenge faced by engineers of AF-reinforced composites.

Various fiber-surface modification methods are used in practice, including chemical grafting [8, 9], chemical etching [10], high-energy irradiation [11, 12], and physical coating [13, 14]. Zhang et al. [15] reported that chemical grafting, especially surface grafting of macromolecular polymers, improves the surface polarity of AFs. AFs grafted with

✉ Le Yang
yangle1990@git.edu.cn

[1] School of Materials Science and Energy Engineering, Guizhou Institute of Technology, Guiyang 550003, China

[2] Guizhou Colleges and Universities Process Industry New Process Engineering Research Center, Guiyang 550003, China

polyvinyl chloride imide exhibited a 40–60-nm thick grafted layer on the epoxy resin matrix and their interfacial shear strength increased by 34% [16]. Prior to chemical grafting modification, AFs must be chemically activated through treatments such as fluorination [17] or complexation [4]. Moreover, the modifier cannot easily graft a uniform interface layer on the fiber surface. Conventional chemical pretreatment methods tend to decrease the fiber strength [18]. Plasma treatment introduces COOH, PH–OH, and other functional groups on the fiber surface with slight damage to the fiber [19–21]. The polyamide acid (PAA) molecule (a polyimide precursor) contains a large number of carboxyl, paramine, and primary amine groups, which can react with corresponding functional groups under heat treatment. Heat treatment stimulates the interface reaction between PAA and AF [18, 22].

Effectively balancing the dispersal, diffusion, penetration, and grafting reaction of a modifier on the fiber surface, which simultaneously occur during the grafting process, is essential for forming a uniform and stable modified layer on the fiber surface. The organic solvents used in the chemical grafting process also affect the modification process and the formation of the grafted layer. Supercritical carbon dioxide ($scCO_2$), with a higher diffusion coefficient and greater permeability than traditional organic solvents, can promote the expansion of molecular chain segments on the fiber surface [23, 24]. Therefore, $scCO_2$ has recently gained traction as an effective solvent in chemical grafting processes. According to Kosareva et al. [25], $scCO_2$ treatment can promote the impregnation and diffusion of the modifier on the fiber surface, and $scCO_2$-assisted grafting modification can improve the thermal stability and interfacial shear strength of modified AFs.

In this study, PAA was synthesized and coated on the surfaces of AFs using $scCO_2$ to promote the chemical reaction between AFs and PAA during the heat treatment process, and hence achieve grafting modification. Finally, styrene butadiene rubber/carbon black/AFs with an SBR/CB/AF ratio of 100/50/2 parts per hundred rubber (phr) composites were prepared. The effect of modification on the interfacial bonding between the modified fibers and SBR was investigated using a rubber processing analyzer and by measuring the dynamic mechanics (DMA), dynamic cutting resistances, and interfacial relative debonding energies of AF/CB/SBR preparations.

2 Experimental

2.1 Materials

Aramid fiber (AF-1000, 1500D) was produced by HYOSUNG Corporation of Korea with the trademark Alkex. The SBR (Model 1502, the styrene content is 23.5% and the M_w is 3.228×10^5 g/mol) was supplied by Dongguan Huanya Rubber Co., Ltd., China. Carbon black (CB, Model N330) was obtained from Wuhan Tanzhan Carbon Black Technology Development Co., Ltd. (China). All rubber auxiliaries, including CB (CB, N330), industrial-grade sulfur (S), stearic acid (SA), diphenylguanidine (D), zinc oxide (ZnO), styrenated phenol (SP-C) as an anti-aging agent, 2-thiolbenzothiazole (M), 2,2′-dithiodibenzothiazole (DM) and tetramethyl thiuram disulfide (TMTD), were provided by Guizhou Tire Co., Ltd. (China).

PAA solution was synthesized using pyromellitic dianhydride (PMDA, AR, Alfa Chemistry Co., Ltd.) and m-phenylene diamine (m-PDA, AR, Alfa Chemistry Co., Ltd.), the molar ratio of monomers was PMDA/m-PDA = 1.02:1. The solid content of PAA solution is 15 wt% and the intrinsic viscosity is 2.78 dL/g. N-Methyl-2-pyrrolidone (NMP, CR, Alfa Chemistry Co. Ltd) was used as a diluent of PAA in the surface modification of aramid fiber.

2.2 Preparation of Modified AFs

Pretreatment process of AFs AF bundles were sheared into segments of length 20 mm. A certain amount of AF was then appropriately dispersed and placed in a blast oven. The oven was rapidly heated to the set 250 °C and the AFs were treated at that temperature for 1 to remove the sizing agent from their surfaces. After 1 h, the fibers were removed and sealed for modification treatment.

Modification of AFs The AFs were modified in a $scCO_2$ reactor (SLM100 instrument; Shenlang Laboratory Instrument Co., Ltd., Beijing, China). The grafting modification process (Fig. 1) was performed at relatively low pressure and temperature (10 MPa, 50 °C, 30 min) to reduce damage to the fiber surfaces by $scCO_2$ as we reported [22]. The treatment processes of samples AF1–AF3 are summarized in Table 1.

2.3 Preparation of Vulcanized Modified AF/SBR Composites

2.3.1 Preparation of Gross Rubber

The auxiliaries were prepared as listed in Table 2. The accurately weighed rubber auxiliaries were mixed with 100 phr of SBR containing 50 phr CB in a two-roll mill (XK-160-A, manufactured by Fujian Yongchun Light Industrial Machinery Factory, China; roller length = 320 cm, roller diameter = 160 cm, speed ratio = 1:1.22). The modified AF content in all composites was fixed at 2 phr (AF/C/SBR = 2/50/100). The gross rubber was synthesized through sequential addition of ZnO, SA, D, SP-C, M, DM, TMTD and 2 phr of the modified

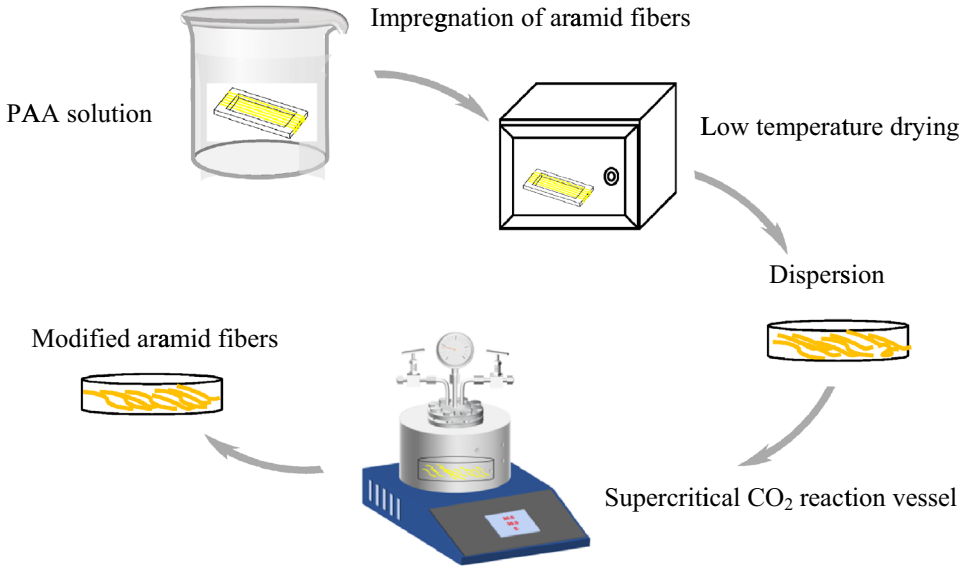

Fig. 1 Schematic of $scCO_2$-assisted grafting modification

Table 1 Treatment processes of the prepared samples

Sample name	Treatment process
AF0	Untreated
AF1	Treatment with $scCO_2$ alone (10 MPa, 50 °C, 30 min) followed by drying
AF2	Soaking in 5% PAA solution at 25 °C for 10 min, followed by drying at 250 °C for 2 h
AF3	Soaking in 5% PAA solution at 25 °C for 10 min, followed by $scCO_2$ treatment (10 MPa, 50 °C , 30 min) and drying at 250 °C for 2 h

Table 2 Formulation of the gross rubber

Components (per 100 rubber)	phr
Styrene butadiene rubber (SBR)	100
Carbon black (CB)	50
Aramid fiber (AF)	2
Zinc oxide (ZnO)	5
Stearic acid (SA)	4
Diphenylguanidine (D)	0.50
2-Mercaptobenzothiazole (M)	2.20
2,2′-Dithiodibenzothiazole (DM)	1.90
Styrenated phenol (SP-C)	1.50
Tetramethylthiuram disulfide (TMTD)	0.32
Sulfur (S)	1.70

fibers. Once the auxiliaries were evenly mixed with the fibers, S was added and mixing was continued for 3–4 min, maintaining the temperature at 40–50 °C. Finally, the roll distance was adjusted to ensure an appropriate thickness of the mixing glue (~2.0 mm), laying a sheet of gross rubber for curing treatment.

2.3.2 Preparation of Vulcanized Rubber

To establish the positive vulcanization time of the AF/C/SBR composites, the flaky mixture was placed in a rotor-free vulcanization instrument (M2000FAN, High Speed Rail Technology Co. Ltd., China) at a temperature of 143.0 °C, a test frequency of = 100.0 cpm, a test time of 10 min, and a rotation angle of 0.5°. The maximum torque (MH), minimum torque (ML), and positive curing time (Tc90) of each group were recorded under these conditions. After measuring the positive vulcanization time, the gross rubber sheet was vulcanized at 145 °C on a press vulcanizer (XLB, 25t, Jiangdu Pearl Experiment Machine Factory, China) for the standard Tc90.

2.4 Characterization Procedures

2.4.1 Characterization of Modified AFs

The surface morphologies of the modified AF fibers were observed using scanning electron microscopy (SEM) (Sirion 200, FEI, USA). The surface chemical compositions of the fibers were analyzed by Fourier transform infrared spectroscopy (FTIR) (Nicolet 8700, Thermo Fisher Scientific, USA) and X-ray photoelectron spectroscopy

(XPS) (Thermo Fisher Scientific) equipped with an Mg–Ka X-ray source and a pass energy of 1486.6 eV. X-ray diffraction (XRD) analyses were performed on a diffractometer (X Pert PRO; Panalytical, province, country) with a scan range of 10°–40° and a scan rate of 2°/min. The tensile strengths of the modified AFs were tested on a single-filament testing device (Shanghai New Fibre Instrument Co. Ltd., XQ-1, China) according to the ASTM-D3379 standard. After collecting 20 effective values, it was confirmed that modification negligibly changed the fiber diameter.

2.4.2 Grafting Rates of Modified Aramid Fibers

To evaluate the grafting rates, the AFs were assessed before and after modification. Prior to grafting, the AFs were dried at 100 °C and the quality was recorded. After modification, the AFs were cleaned several times in acetone and dried at 100 °C in the oven. The change in quality between the modified and unmodified AFs was defined as the grafting amount of modified AF.

2.4.3 Characterization of Vulcanized Rubber

The dynamic mechanical properties of the vulcanized rubber were measured on a dynamic mechanical analyzer (Q800, TA; USA). During this test, the frequency and amplitude were set to 1 Hz and 8 μm, respectively. The mechanical properties of the vulcanized rubber composites were evaluated on a universal material tester (WdW-10c, Shanghai Hualong Test Instrument Co. LTD, China) under the ISO 37-2005 and ISO 34-1-2010 (right angle) standards. The vulcanized rubber was tested on a rubber processing analyzer (RPA2000, Alpha Technology Co., Ltd., USA) at 1 Hz. The strain-scanning range is 0.1 ~ 450%. The dynamic cutting performance test was conducted at 120 times/min with a stroke of 48 ± 1 mm. The loss mass from the rubber wheel was recorded every 2 min and the fracture morphology of the vulcanized rubber was observed by SEM (Sirion 200, FEI).

3 Results and Discussion

3.1 XPS Analysis

Figure 2 and Table 3 present the surface element contents of the untreated and modified fibers. Changes in AF0 and AF1 have been reported in our previous studies and are reproduced for intuitive comparison [22, 24]. The C 1 s core-level spectrum of the proto-filament displays the signals of C=C, C–C, C–N, and C=O (Fig. 2). Differently, there exist five peaks in the C1s spectrum for AF1, which correspondingly originate from C=C (284.6 eV), C–C (285.3 eV), C–N (286.2 eV), C=O (286.7 eV), and –COO– (289 eV) groups on the macromolecular chain [22, 26]. The content of –COO– on the fiber surface reached 1.4% (in Table 3), and the appearance of –COO– confirmed that the near-range interaction between supercritical CO_2 and C=O of aramid fiber made it easier for CO_2 to diffuse into the fiber interior [24, 27]. The –COO– content increased to 2.8% after modification with PAA (AF2) and to 3.1% after $scCO_2$-assisted PAA grafting (AF3). Besides confirming the grafting reaction, the presence of –COO– demonstrates that the –COOH groups of PAA were not completely aminated at the test temperature (250 °C). These oxygen-containing groups enhanced the polarity of the fibers, benefitting interfacial adhesion between the modified fibers and the matrix.

3.2 FTIR and Graft Rate Analyses

The graft reaction is hindered by the high crystallinity of the molecular chains on the AF surface. The FTIR spectra and grafting rate analysis confirm the effectiveness of the PAA grafting reaction (Fig. 3). The FTIR spectrum of AF0 presents the characteristic peaks of $–CH_2–$ at 2923 and 2856 cm^{-1}, which derive from the sizing agent on the fiber surface (Fig. 3a). The sizing agent disappeared under the combined action of $scCO_2$ and heat treatment on the modified fibers [28]. The benzene-ring absorption peak at 1610 cm^{-1} slightly changed after modification, indicating oxidation of the molecular chains on the fiber surface during the heat treatment. The spectra of AF2 and AF3 present the characteristic absorption peaks of PAA at 1716 and 1775 cm^{-1}. Accompanied with the heat treatment process, hydrogen bonds formed between PAA and a large number of carboxyl group, amino group on the fiber surface, –COOH on the fiber surface were involved in the imidization of PAA molecular chains, the absorption peak of 3314 cm^{-1} also gradually weakened [29, 30]. Figure 4 is a schematic of the interface reaction. The graft reaction of the untreated fibers (AF0) yielded 0.029 g of coatings per gram of AF0, below the concentration of the PAA solution (5%). Although there are very few polar functional groups on the surface of aramid fiber, the self-polymerization of PAA is inevitable. For untreated neat AF(AF0), the grafting rate was 2.88%. After $scCO_2$ treatment, the fiber surface loosened and the PAA easily penetrated, enhancing the grafting rate to 6.84%. Meanwhile, $scCO_2$-assisted grafting boosted the surface grafting rate to 10.23%, further proving that $scCO_2$ promotes the formation of grafted materials in the grafting process. Figure 3c presents the thermogravimetric curves of each sample. According to Fig. 3c, the mass residue rate of AF0 is 48%, while that are 50, 52, and 57% for AF1, AF2, and AF3, respectively. These values are basically consistent with the test data of graft rate in Fig. 3b.

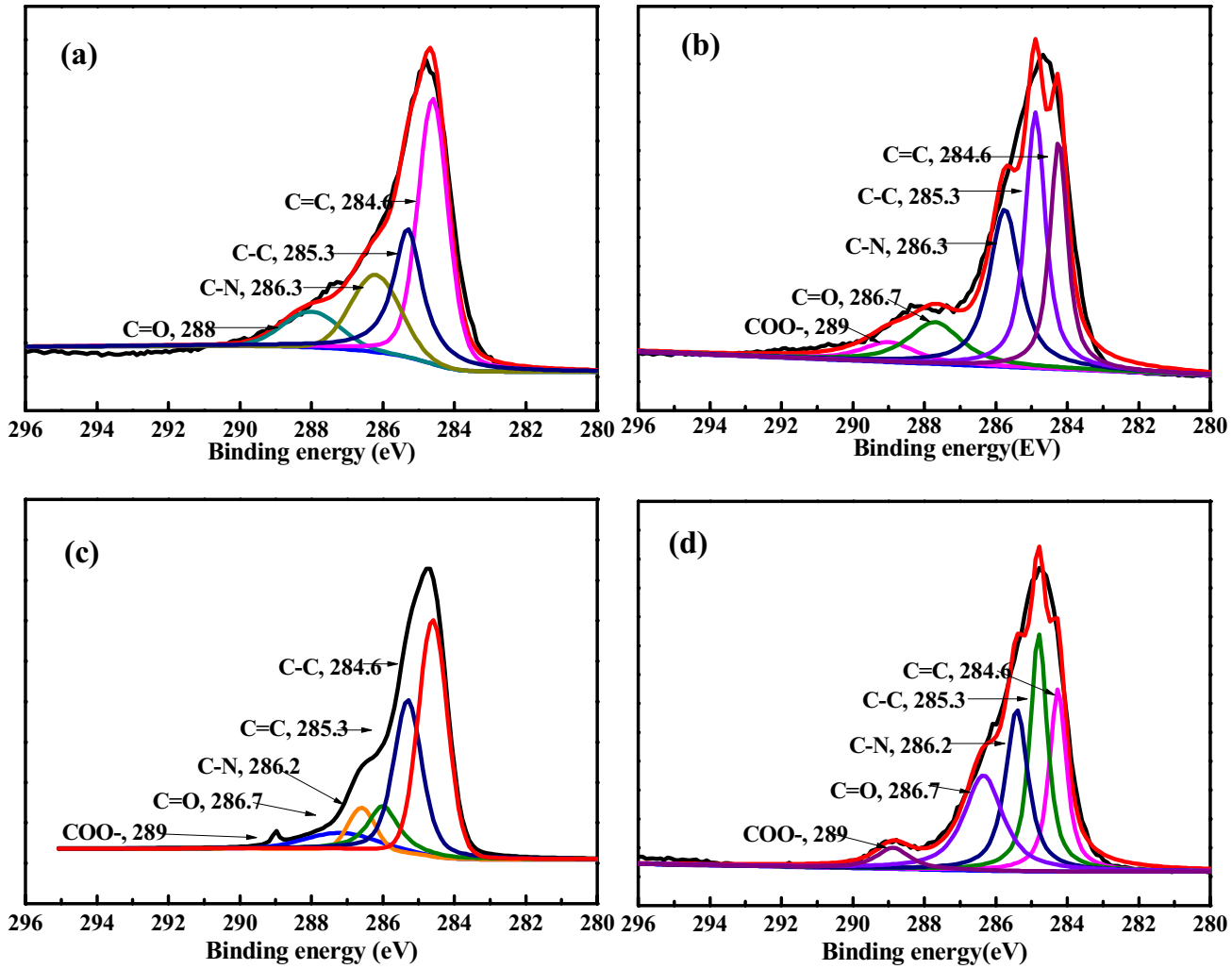

Fig. 2 C 1 s core-level spectra of **a** the unmodified aramid fibers (AF0) and modified fibers, **b** AF1, **c** AF2, and **d** AF3 (see Table 1 for the modification processes)

Table 3 Relative chemical compositions of the unmodified and modified AFs

Samples	C–C and C=C	O=C–N–H (C=O, C–N)	–COO–
AF0	88.15	11.85	0
AF1	76.87	21.73	1.4
AF2	78.93	18.27	2.8
AF3	78.56	18.34	3.1

3.3 Microscopic Morphology Analysis

As is well known, grafting modification forms grafted attachments that roughen the fiber surface, facilitating its interfacial locking with many matrix materials. Changes in AF0 and AF1 have been reported in our previous studies and are reproduced for intuitive comparison [24]. Figure 5 presents SEM images of the AF0, AF1, AF2, and AF3 samples. AF0 and AF1 present similarly smooth and clean surfaces, indicating that $scCO_2$ as an auxiliary process does not damage the fibers [31]. After PAA grafting to form AF2, a continuous flaky structure with small grains appeared on the fiber surface, indicating the grafting of PAA and the desired surface roughening of the fiber surface. In addition, the layer grafted on the fiber surface was clearly more uniform and compact after $scCO_2$-assisted PAA modification to form AF3.

3.4 Aggregate Structure and Tensile Strength Analysis of the Modified Fibers

Permeation and grafting of the modifier exert non-negligible influences on the aggregate structures of AFs during chemical grafting modification. Figure 6a displays the XRD patterns of the AFs under different treatment conditions. The

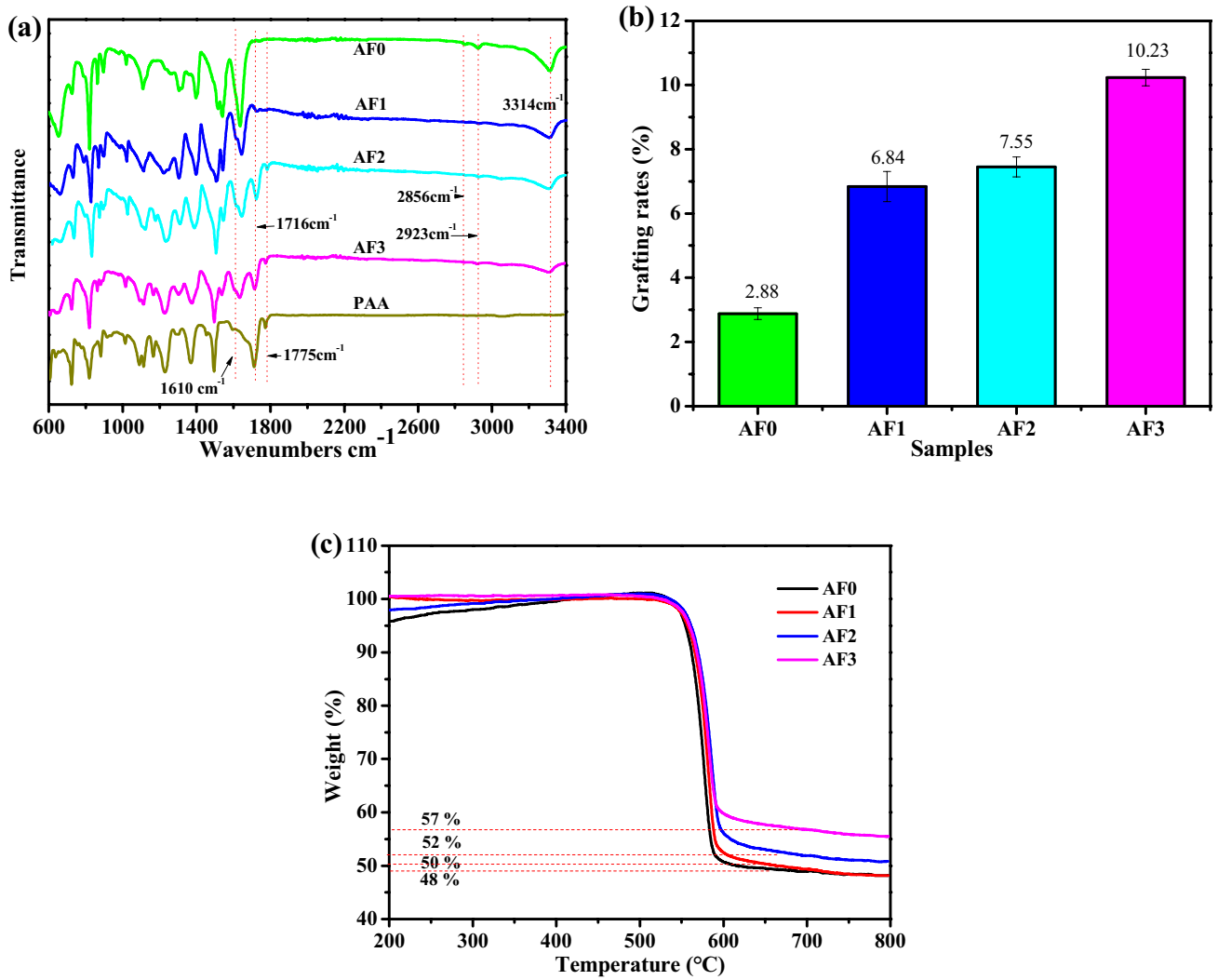

Fig. 3 **a** FTIR spectra, **b** grafting rates, **c** TG of the unmodified and modified AFs

characteristic diffraction peaks at 20.74° and 23.05° belong to the (110) and (200), respectively. These peaks appear in the spectra of each sample, indicating that modification largely preserves the crystallographic texture of the AFs [32]. Table 4 gives the data derived from the peak area of each curve, determined through curve fitting and normalization. Under the action of $scCO_2$, the molecular chain segments on the AF-surface layer move more easily along the fiber axis than along the radial direction. The radial arrangement of the segments corresponds to the (110) crystal plane, which displays an enhanced diffraction peak after $scCO_2$ modification (Fig. 6a). Modification increased the interplanar spacing and reduced the stacking density of the microcrystals; correspondingly, the 2θ values of the (110) and (200) planes slightly shifted to smaller angles. Hydrogen bonds formed between PAA and a large number of carboxyl and amino groups on the fiber surface, while the –COOH groups on the fiber surface were involved in the imidization of PAA molecular chains [33]. The crystallinities of the AF2 and AF3 modified fibers are 81.59 and 82.74%, respectively, 7.13 and 8.64% higher than that of AF0, respectively.

3.5 Frequency-Scanning Analysis of Gross Rubber

Figure 7 shows the elastic behavior–frequency curves of the modified AF/CB/SBR (2/50/100 phr). The energy storage moduli G' and loss moduli G'' gradually increased with increasing frequency. At any given frequency, the G' and G'' values were higher in the modified AFs/CB/SBR gross composites than in the AF0/CB/SBR gross composites and higher in the AF3/CB/SBR gross composites than in all other gross composites. These results indicate that $scCO_2$ treatment improves the bonding between the grafted layer on the modified fiber and SBR matrix; therefore, the grafted

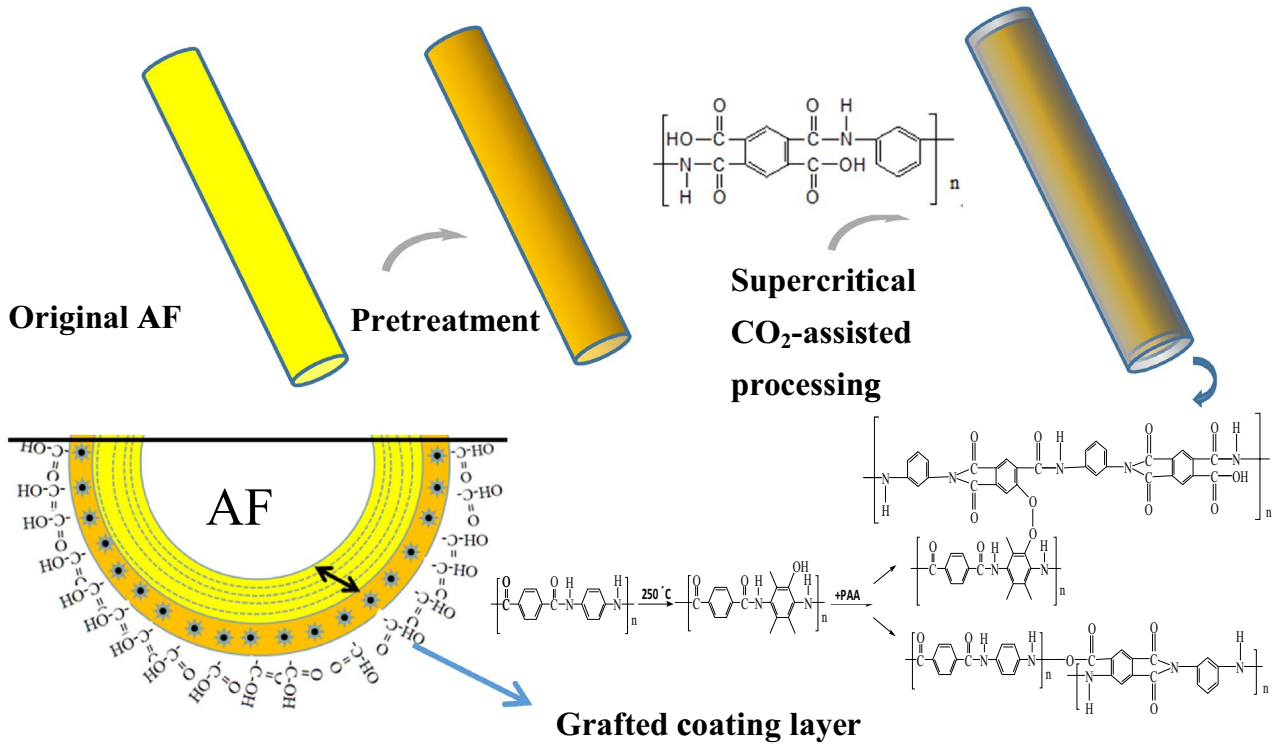

Fig. 4 Schematic showing the interface reaction of AF modification

layer remains stable and intact during the high-shear rubber mixing process. Meanwhile, the loss factor (tan δ) decreased with increasing frequency (Fig. 7c) and was highest in the AF3/CB/SBR gross composites, indicating that improving the interfacial adhesion between the modified fibers and SBR increases the internal friction during frequency scanning [34].

3.6 Machining Properties and DMA Analysis of the Vulcanized AF/CB/SBR Composites

The characteristic vulcanization data of the modified AF/CB/SBR composites are shown in Fig. 8a. The cross-linking density of the composites can be measured as the difference between the MH and ML of the compound (i.e., MH–ML) [4]. After modification, the interface layer grafted on the fiber surface promoted the dispersion of vulcanization agents to the fiber surface during the mixing process and stabilized the vulcanization network around the fiber. The MH–ML value was much larger in AF3/CB/SBR than in the other samples, indicating a more obvious cross-linking density increase in AF3/CB/SBR than in the other samples.

Figure 8b displays the loss factors of the composites. According to Ashida et al. [35], the interfacial adhesion of fiber-reinforced composites can be calculated as

$$\tan\left(\delta_{\max}\right) = \tan(\delta_{\max})_m - \alpha\varphi_{\mathrm{f}},$$

where φ_{f} is the volume fraction of fibers, α is the interfacial adhesion parameter, and $\tan(\delta_{\max})$ and $\tan(\delta_{\max})_{\mathrm{m}}$ are the loss factors of the modified AF/CB/SBR and CB/SBR composites, respectively. As $\tan(\delta)$ of the CB/SBR composites is constant, a lower $\tan(\delta)$ of AF/CB/SBR corresponds to stronger interfacial adhesion. The lower $\tan(\delta)$ of AF3/CB/SBR than of the other composites was, therefore, attributed to the stronger interfacial adhesion between rubber and AF3 than between rubber and the other modified fibers. PAA alone adhered to the fiber surfaces of AF2, which was not treated with supercritical CO_2. During high-shear mixing, PAA is easily detached from the fiber surface and enters the rubber matrix. Moreover, as PAA is an acidic substance, it decreases the cross-linking density in the cross-linked network; consequently, the $\tan(\delta)$ of AF2/CB/SBR shifted toward the lower temperature zone.

3.7 Strain-Scanning Curves of the Vulcanized AF/CB/SBR Composites

Figure 9 shows the strain-scanning curves of the modified vulcanized composites. Vulcanization formed the cross-linking networks in the composites. In the small strain area, the storage moduli (G') of the vulcanized composites were independent of strain and differed only because the

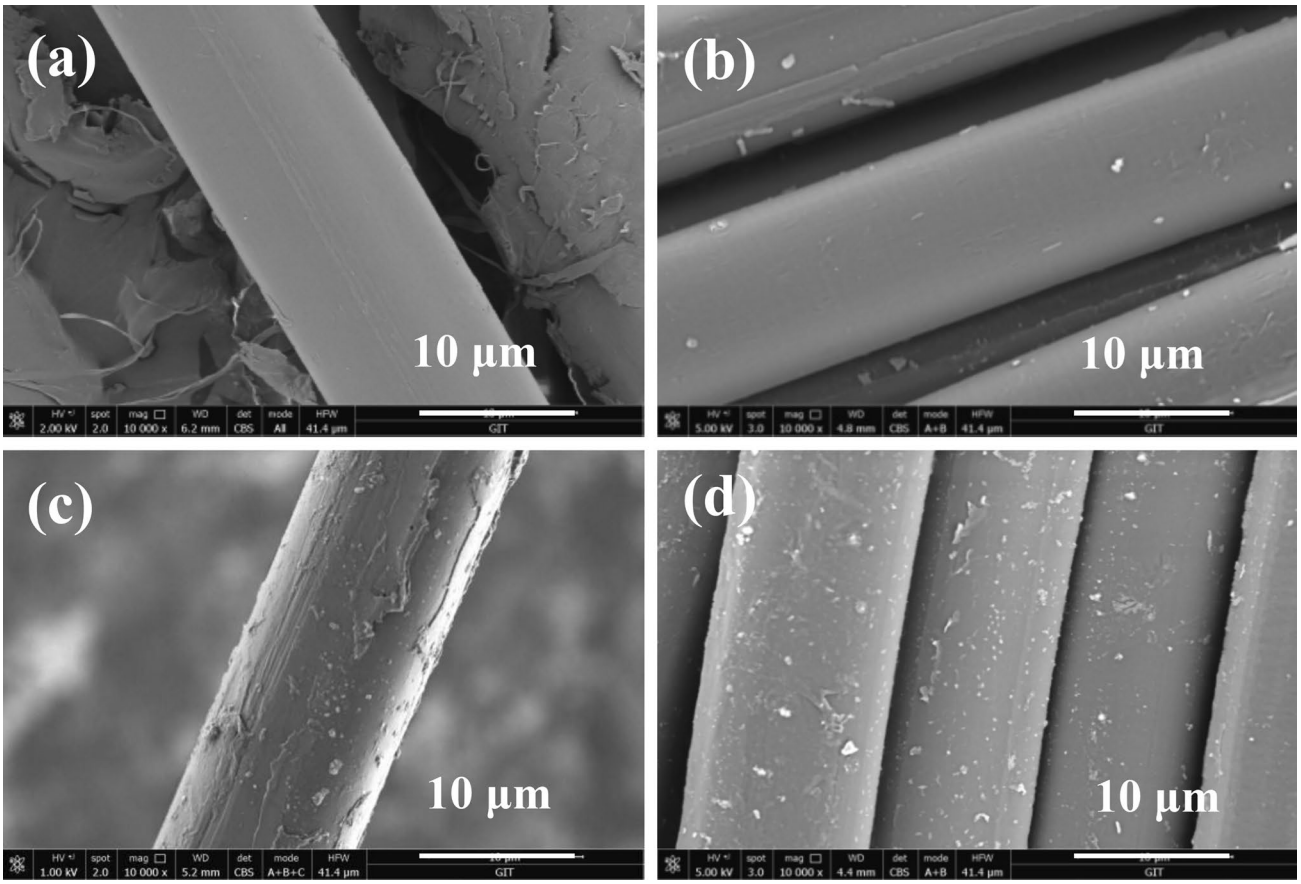

Fig. 5 SEM images of **a** the unmodified aramid fibers (AF0) and the modified fibers **b** AF1, **c** AF2, and **d** AF3

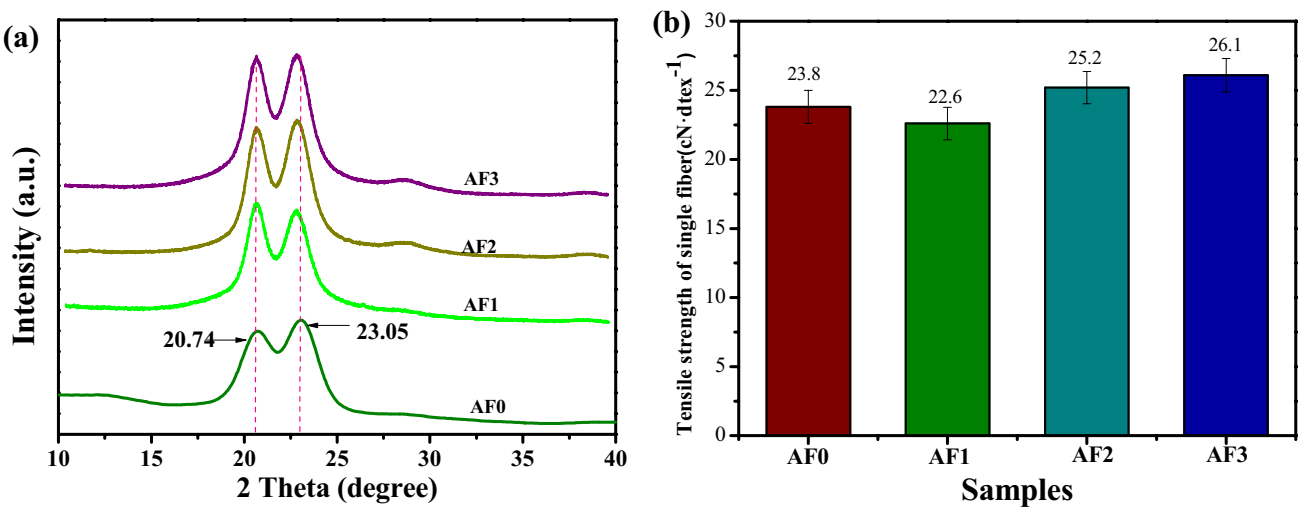

Fig. 6 **a** XRD patterns and **b** tensile strengths of mono-filaments of the unmodified and modified AFs

surfaces of the modified fibers carried different grafted layers. Relative to CB/SBR, the G' and G'' were more obviously increased in AF3/CB/SBR than in AF1/CB/SBR and AF2/CB/SBR, indicating that $scCO_2$-assisted PAA modification increased the rigidity of the interface layer on the modified fiber surface, blocking the movement of rubber molecules under the shear force. The high G' and G'' can be explained by the difficulty of relative

Table 4 Comparison of crystallinity structure parameters of the modified AFs

Samples	2θ (°)		d (Å)[a]		FWHM (°)[b]		X_s[c] (nm)	X_c[d] (%)
	(110)	(200)	(110)	(200)	(110)	(200)		
AF0	20.74	23.05	4.2787	3.8544	1.629	1.699	5.4	76.16
AF1	20.68	22.77	4.2842	3.8722	1.481	1.520	5.6	79.56
AF2	20.56	22.87	4.3048	3.8823	1.413	1.531	5.7	81.59
AF3	20.51	22.68	4.3077	3.8942	1.466	1.517	5.7	82.74

[a]Interplanar spacing

[b]Peak width at half height

[c]Average crystallite size

[d]Crystallinity

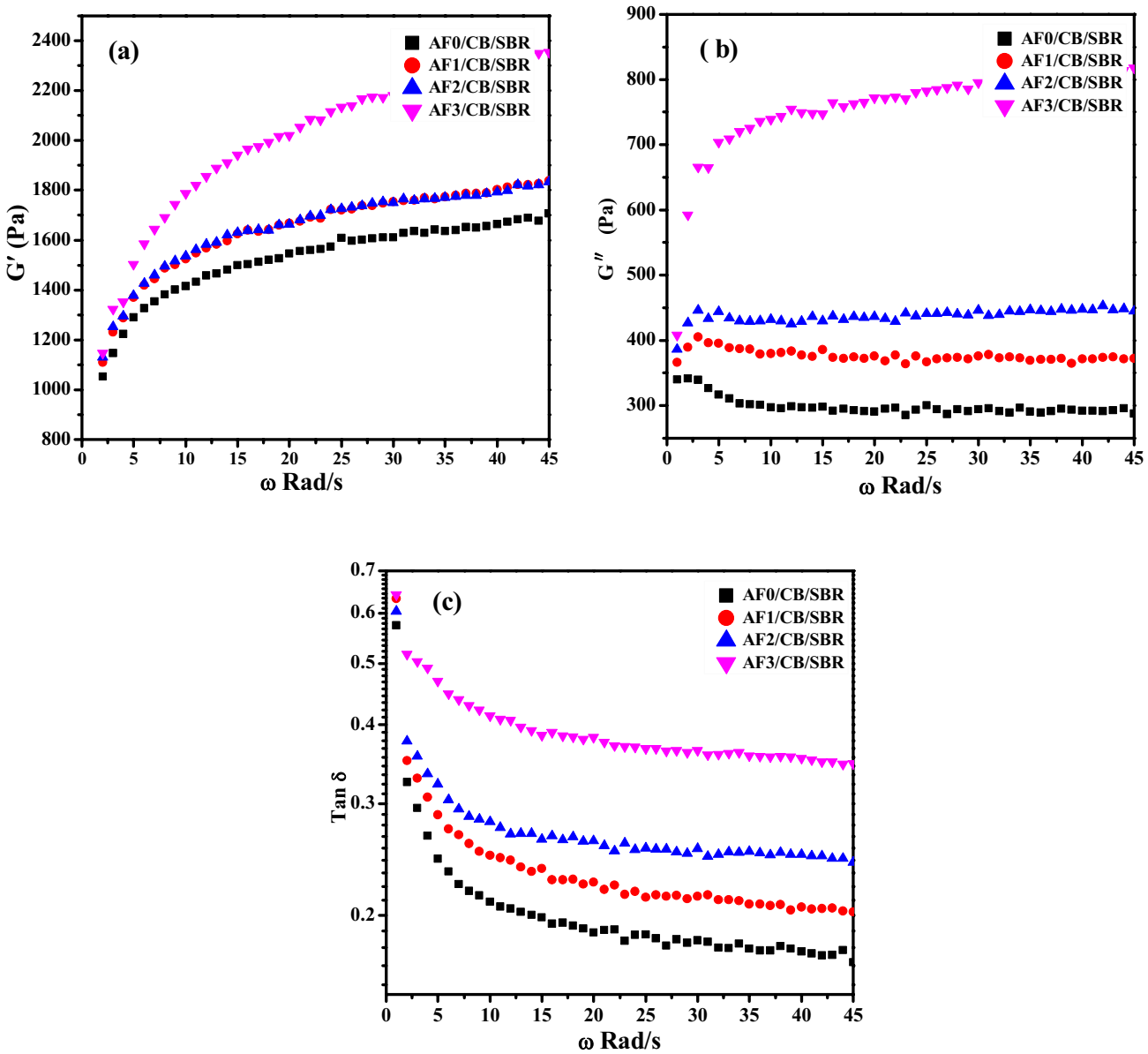

Fig. 7 Frequency-scanning curves of the modified AF/CB/SBR gross rubber composites: **a** energy storage moduli; **b** loss moduli; **c** loss factors

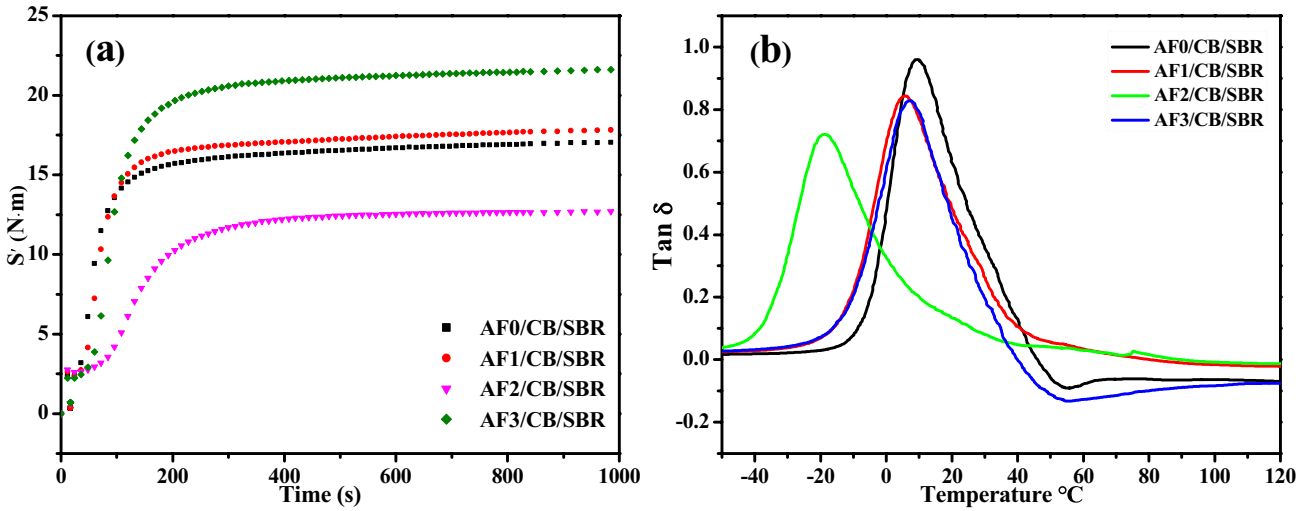

Fig. 8 **a** Machining properties and **b** DMA analysis of the vulcanized AF/CB/SBR composites

slippage between the molecules and the increased interaction between the modified fibers and CB in the vulcanized composites. The cross-linking network formed in the vulcanized rubber greatly reduced the viscosity of the composites. As the improvements of G' and G'' on the surface interface layers of the modified fibers were well balanced, the tan(δ) values did not obviously differ among the composites.

3.8 Mechanical Properties of the AF/CB/SBR Vulcanized Composites

Figure 10 shows the mechanical properties of the modified AF/CB/SBR composites. Modification slightly changed the tensile strengths of the composites and notably increased their moduli at 100% and tear strength in Fig. 10c, d. Raw strain–stress curves of each samples are provided in Fig. 10a. Judging from this finding, the polarity of the fiber surfaces plays no dominant role in improving the tensile strengths of the composites. After $scCO_2$-assisted PAA modification, the –COOH groups in the grafted layer on the fiber surface can participate in the curing process. In addition, the uniformly grafted layer with high toughness can evenly transfer an applied stress along the fiber, thereby improving the comprehensive performance of the fiber-reinforced composites. The tensile strength and modulus at 100% of the AF3/CB/SBR composites were 16.01 and 32.47% higher, respectively, than those of AF0/CB/SBR in Fig. 10b. AF2/CB/SBR also exhibited improved mechanical properties, but its grafted layers were non-uniform and its stability was poor during high-shear rubber processing. Only AF3/CB/SBR exhibited an obvious improvement in comprehensive properties.

3.9 Cutting Resistance Analysis

Figure 11 plots the cutting resistances of the differently treated AF/CB/SBR vulcanized rubbers (AF/CB/SBR = 2/50/100 phr) as functions of time. Stronger crack-growth and cutting resistances in vulcanized rubber indicate stronger interfacial bonds between the modified fibers and SBR matrix [36]. The cutting resistances of the modified AF/CB/SBR composites were notably improved from that of AF0/CB/SBR. However, after $scCO_2$ treatment, AF dispersion through the rubber was facilitated by the roughness and uniformity of the grafted layer. The large energy absorption of crack propagation further improved the anti-cutting performance of AF3/CB/SCR.

3.10 SEM Analysis of Modified AF/CB/SBR Vulcanized Composites After Tensile Fracture

Figure 12 shows SEM images of tensile fractures in the modified AF/CB/SBR vulcanized composites. The adhesion between the proto-filament (AF0) and SBR was poor, and pulled-out fibers appeared at the fracture site of the

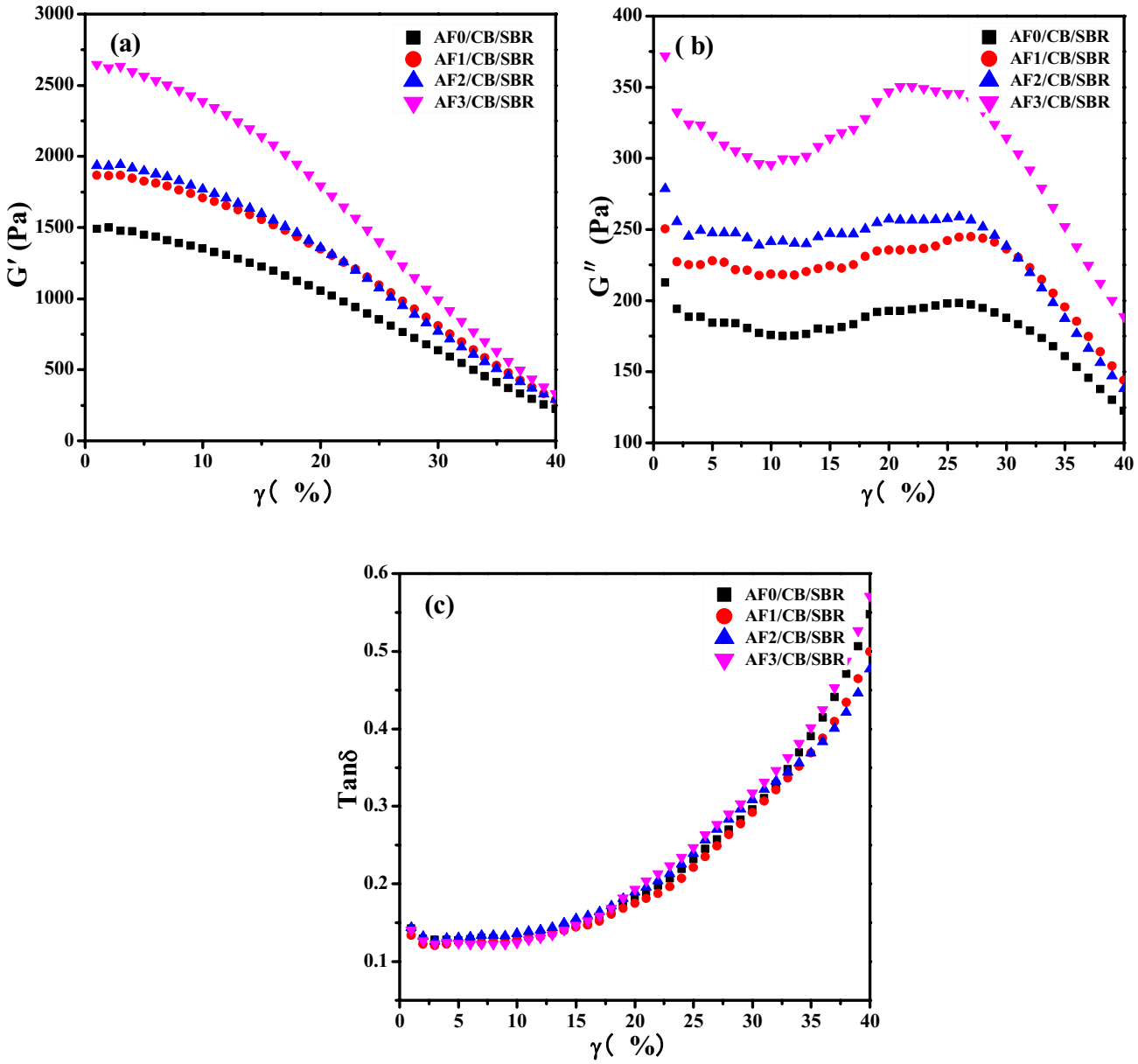

Fig. 9 Strain-scanning curves of the modified AF/CB/SBR vulcanized composites: **a** energy storage modulus; **b** loss modulus; **c** loss factors

AF0/CB/SBR vulcanized composite; moreover, the fiber surface is relatively smooth. After modification, the interfacial adhesion between the fibers and SBR matrix slightly improved and fiber avulsion appears in the SEM images of AF1/CB/SBR and AF2/CB/SBR. $ScCO_2$-assisted PAA modification further improved the interface adhesion between the uniformly grafted layer and SBR matrix rubber and almost all fibers were torn during the stretching process, indicating higher fiber strength in this composite than in the other composites.

4 Conclusion

In this study, AFs were modified at a high grafting rate through $scCO_2$-assisted PAA grafting modification. $ScCO_2$ assistance facilitated the diffusion, penetration, and grafting reaction of PAA, achieving not only an excellent grafting rate but also a uniformly grafted layer on the modified fibers. The amino and carboxyl groups in the PAA molecules reacted with the polar AFs and participated in hydrogen-bond formation. After $scCO_2$-assisted grafting with

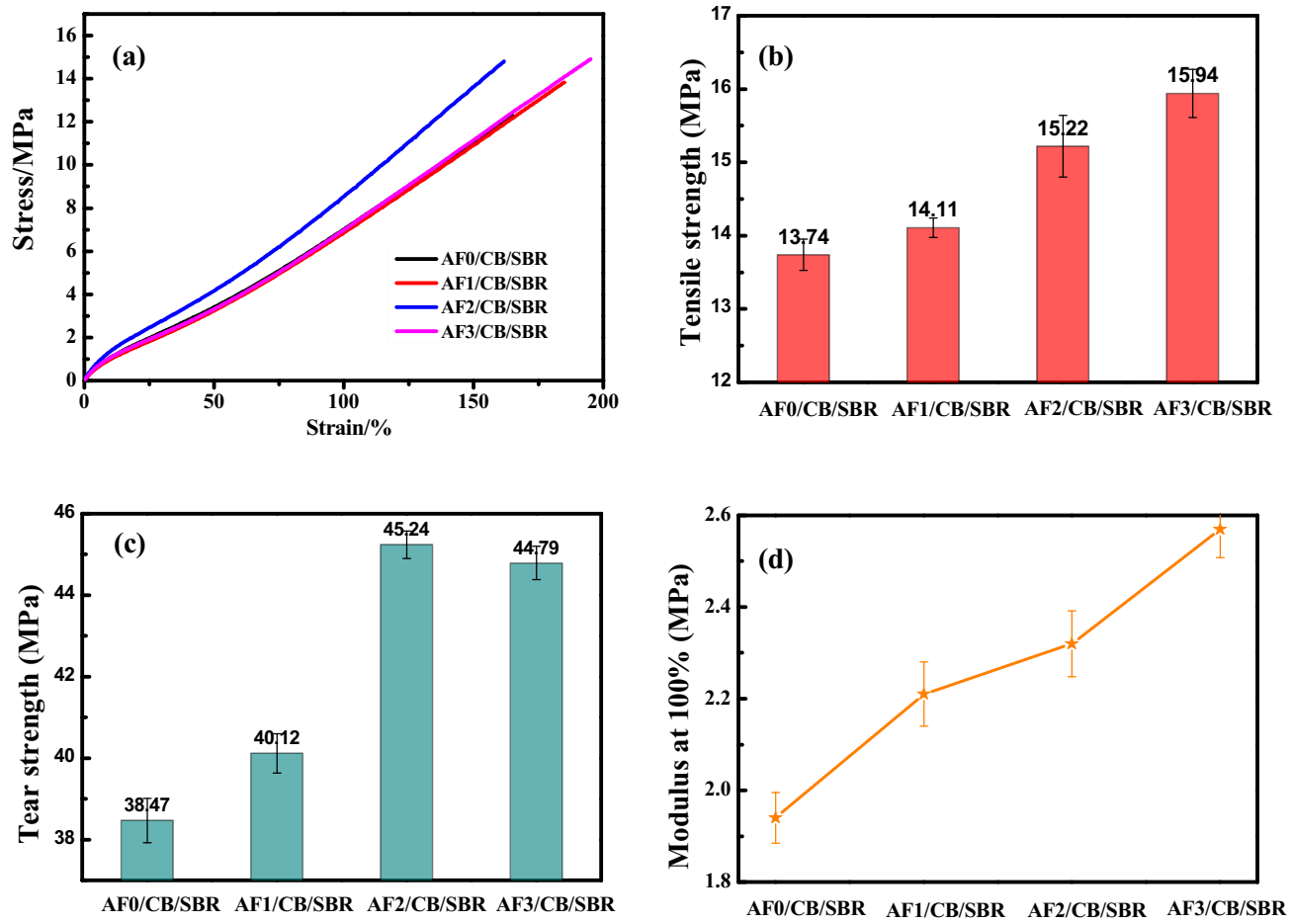

Fig. 10 Mechanical properties of the modified AF/CB/SBR vulcanized composites: **a** stress–strain curve; **b** tensile strength; **c** tear strength; **d** modulus at 100%

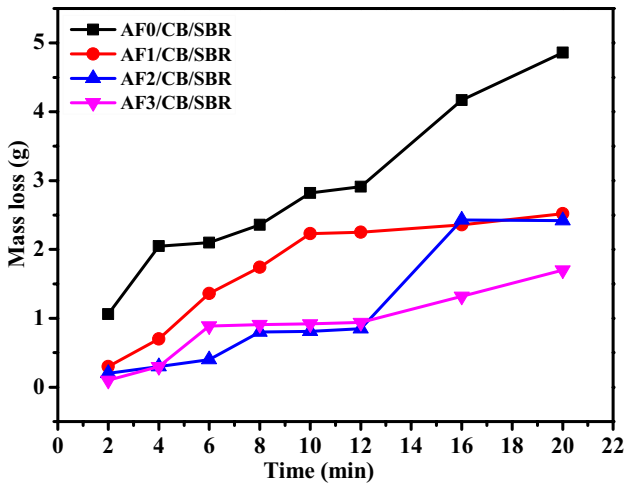

Fig. 11 Cutting resistance plots of the AF/CB/SBR vulcanized rubbers

5 wt% PAA, the grafted amount was 10.23%, the surface crystal spacing increased, and the crystallinity increased by 8.64%. As an acidic substance in the grafted layer, PAA delayed the vulcanization process and increased the positive vulcanization time. Moreover, the –COOH groups in the grafted surface layer could participate in the curing process of the curing agent, increasing the energy storage and loss moduli of the gross and vulcanized composites. In AF3/CB/SBR, the tensile strength and modulus at 100% were 16.01% and 32.47% higher, respectively, than those of AF0/CB/SBR, and the cutting resistance improved accordingly. This study widens the application of $scCO_2$ as an auxiliary process during AF-surface modification and provides a feasible method for fabricating modified AF-reinforced rubber composites with excellent performance.

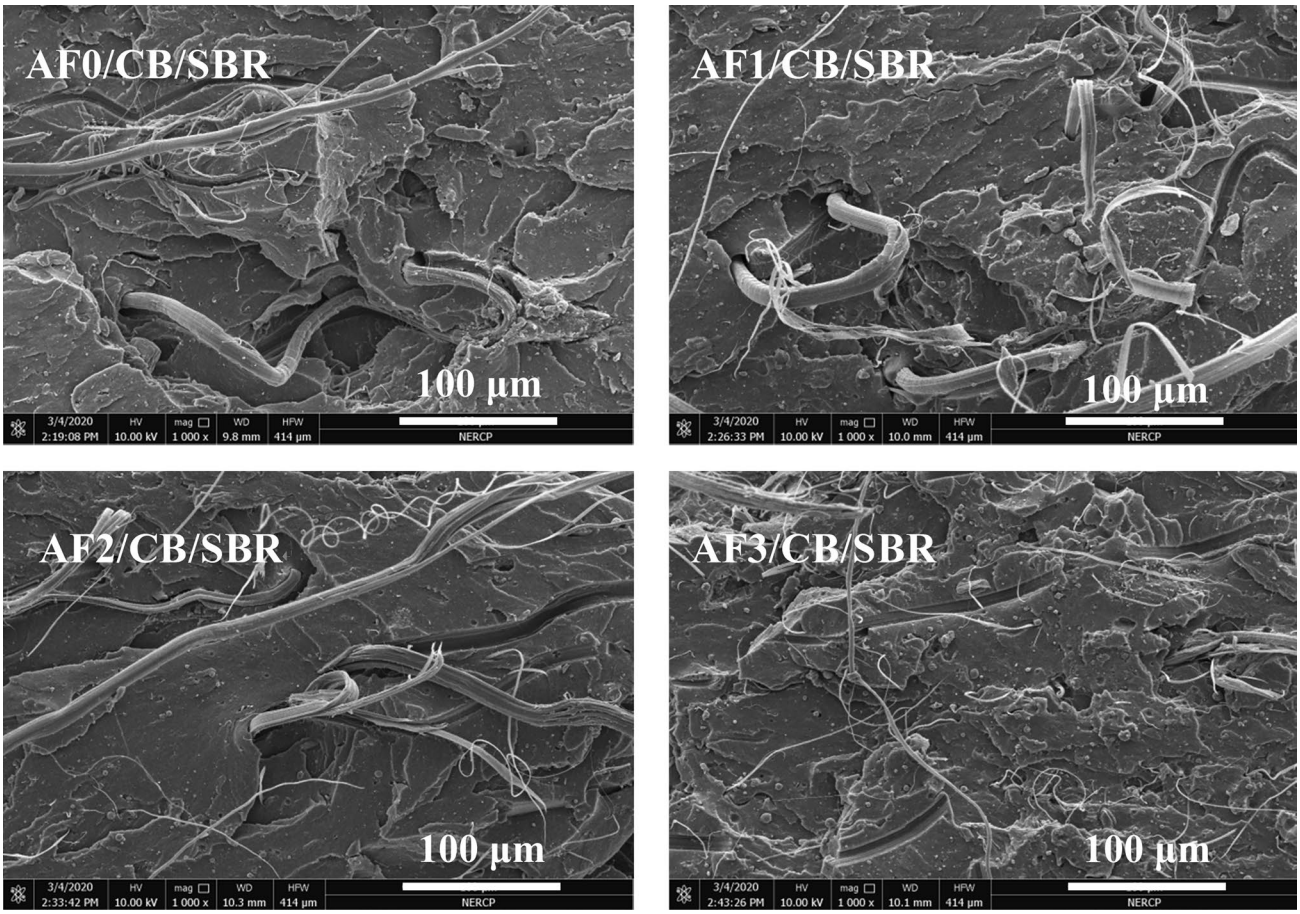

Fig. 12 SEM images of the modified AF/CB/SBR vulcanized composites after tensile fracture

Acknowledgements The authors gratefully acknowledge the National Natural Science Foundation of China (grant No. 52363009), Guizhou Institute of Technology high-level talent launch project, Guizhou Colleges and Universities Process Industry New Process Engineering Research Center (Qian Jiao Ji [2022] 034).

Author contributions Yang Li: conceptualization, methodology, investigation, writing—original draft; Caiwen Shi: resources, methodology. Xiaoli Pan: conceptualization, investigation. Le Yang: investigation.

Funding National Natural Science Foundation of China, 52363009, Yang Li.

Data availability The data that support the findings of this study are available from the corresponding author upon reasonable request.

Declarations

Conflict of interest The authors declare no conflict of interest.

References

1. W. Du, J. Zhang, Z. Zhao, X. Zhang, Compos. Commun. **22**, 100438 (2020)
2. X.Y. Gong, Y.Y. Liu, M. Huang, Q.L. Dong, N. Naik, Z.H. Guo, Compos. Commun. **29**, 100996 (2022)
3. A. Gosar, M. Nagode, S. Oman, Fatigue Fract. Eng. Mat. Struct. **42**, 307 (2019)
4. L.P. Yin, Z.T. Zhou, Z. Luo, J.C. Zhong, P. Li, B. Yang, L. Yang, Polym. Test. **80**, 106092 (2019)
5. J.C. Zhong, Z. Luo, Z. Hao, Y.L. Guo, Z.T. Zhou, P. Li, B. Xue, Compos. B Eng. **172**, 485 (2019)
6. Z. Cheng, H. Wu, T.J. He, J.Q. Qin, X.Y. Liu, Compos. B Eng. **182**, 107608 (2020)
7. Z. Cheng, L.J. Zhang, C. Jiang, Y. Dai, C.B. Meng, L.B. Luo, X.Y. Liu, Chem. Eng. J. **347**, 483 (2018)
8. J.W. Lv, Y.H. Liu, Y.T. Qin, Q. Yin, S.Y. Chen, Z. Cheng, J.Y. Yin, Y. Dai, Y. Liu, X.Y. Liu, Compos. A **145**, 106386 (2021)
9. C. Yang, H. Wu, Y. Dai, S.Y. Tang, L.B. Luo, X.Y. Liu, Polymer **180**, 121687 (2019)
10. G.Y. Lin, H. Wang, B.Q. Yu, G.K. Qu, S.W. Chen, T.R. Kuang, K.B. Yu, Z.N. Liang, Mater. Chem. Phys. **255**, 123486 (2020)
11. H. Yuan, W.C. Wang, D. Yang, X.F. Zhou, Z.L. Zhao, L. Zhang, S. Wang, J. Feng, Surf. Coat. Technol. **344**, 614 (2018)
12. W. Mengjin, J. Lixia, L. Suling, Q. Zhigang, W. Sainan, Y. Ruosi, Surf. Interfac. **24**, 101077 (2021)
13. B. Zhang, T. Lian, X. Shao, M. Tian, N. Ning, L. Zhang, W. Wang, Ind. Eng. Chem. Res. **60**, 2472 (2021)
14. S.H. Zhang, M.Z. Li, K. Cheng, S.J. Lu, Colloids. Surf. A. **589**, 124426 (2020). https://doi.org/10.1016/j.colsurfa.2020.124426

15. B. Zhang, L.H. Jia, M. Tian, N.Y. Ning, L.Q. Zhang, W.C. Wang, Eur. Polym. J. **147**, 110352 (2021)
16. Z. Cheng, C. Chen, J.Y. Huang, T. Chen, Y. Liu, X.Y. Liu, Appl. Surf. Sci. **401**, 323 (2017)
17. J.W. Lv, Z. Cheng, H. Wu, T.J. He, J.Q. Qin, X.Y. Liu, Compos. B Eng. **182**, 107608 (2020)
18. Y. Li, Z. Luo, L. Yang, Y.M. Luo, Q. Li, L.Y. Zhang, K. Xiang, Polymer **178**, 121550 (2019)
19. W.T. Sun, W.L. Zhou, J. Mater. Res. Technol. **8**, 4705 (2019)
20. L.X. Zhao, W.Z. Liu, M. Xu, Y. Huang, Q. Zheng, S. Sun, Y. Wang, Plasma Process. Polym. **16**, 1900114 (2019)
21. J.Y. Chen, L.H. Zhao, K. Zhou, Addit. Manuf. **51**, 102576 (2022)
22. Y. Li, G.Y. Xie, R. Li, Y.J. Wu, C.Q. Chen, Z. Luo, J. Mater. Res. Technol. **21**, 1 (2022)
23. P.H. Chen, C.-P. Iun, J.-C. Tsai, M. Tang, J. Supercrit. Fluids **186**, 105589 (2022)
24. Y. Li, C.W. Shi, X.L. Pan, L. Yang, C. Zhang, Polym. Int. (Early View) (2024). https://doi.org/10.1002/pi.6613
25. E.K. Kosareva, M.N. Zharkov, D.B. Meerov, R.V. Gainutdinov, I.V. Fomenkov, S.G. Zlotin, A.N. Pivkina, I.V. Kuchurov, N.V. Muravyev, Chem. Eng. J. **428**, 131363 (2022)
26. F. Tang, Y.G. Jeong, Compos. A **171**, 107558 (2023)
27. C. Zhang, Y.X. Jiang, J.P. Sun, H. Xiao, M.W. Shi, J.J. Long, J. CO2 Util. **37**, 85 (2020)
28. Z.Y. Liu, C.J. Xie, X.L. Tuo, Mater. Today Commun. **31**, 103376 (2022)
29. F. Sohbatzadeh, E. Shakerinasab, S. Mirzanejhad, Polym. Test. **117**, 107836 (2023)
30. Z.Q. Lu, B. Geng, Q. Ma, D.D. Ning, R.X. Zhao, F.G. Kong, E. Songfeng, Appl. Surf. Sci. **607**, 155045 (2023)
31. H.F. Li, Y. Xu, T. Zhang, K.M. Niu, Y. Wang, Y.Q. Zhao, B.M. Zhang, Polym. Test. **81**, 106209 (2020)
32. X.Y. Kong, X. Geng, S.G. Geng, R.J. Qu, Y. Zhang, C.M. Sun, J.F. Wang, Y. Wang, C.N. Ji, Surf. Interfaces **30**, 101922 (2022)
33. S. Feng, Q. Ma, J.Z. Huang, Z.F. Jin, Z.Q. Lu, Compos. A **137**, 106031 (2020)
34. L.P. Yin, Z. Luo, J.C. Zhong, B. Yang, Y.C. Ji, Int. J. Fatigue **134**, 105502 (2020)
35. M. Ashida, T. Noguchi, S. Mashimo, J. Appl. Polym. Sci. **30**, 1011 (1985)
36. S. Saha, K. Vineet, A.K. Bhowmick, A. Saha Deuri, D.M. Vaidya, Polym. Test. **94**, 107048 (2021)